13th ewtec 2019 Proceedings of the 13th European Wave and Tidal Energy Conference 1-6 Sept 2019, Naples, Italy

Hydroelastic modelling of flapping foils operating as flow and wave energy devices

Dimitra E. Anevlavi, Evangelos S. Filippas, Angeliki E. Karperaki and Kostas A. Belibassakis

Abstract— **The performance of oscillating hydrofoils in the presence of waves and currents is studied for the exploitation of combined renewable marine energy sources in nearshore and coastal regions. In the present work, a hydro-elastic model is proposed for the investigation of the effects of chord-wise flexibility on the performance of flapping foils, whose structural response is actuated by an unsteady pressure field generated by the prescribed harmonic motion of the hydro-mechanical system. A fluid-structure interaction solver has been developed to simulate the time-dependent structural response of the oscillating hydrofoil. The solver couples a low-order boundary element method (BEM) for the unsteady hydrodynamics with an finite element method (FEM) for the cylindrical bending of thin elastic plates, based on the classical Kirchhoff-Love theory. The proposed scheme is validated with experimental data and numerical results concerning the performance of the system over a range of design parameters, including Strouhal number, heaving and pitching amplitudes, are presented. The results show that incorporating flexural rigidity profile variations and allowing chord-wise deformations to occur, enhances the performance of these systems. Finally, the present model after enhancement could serve as a useful tool in the design, assessment and control of biomimetic systems for renewable energy extraction.**

Keywords—**Fluid-structure interaction, flapping foils, flexibility effects, Boundary Element Methods, Finite Element Analysis.**

I. Introduction

THE mutual existence of waves with strong following, oblique or opposing currents at various nearshore locations, which are otherwise characterized by quite low wave potential, offers motivation for the development of hybrid technological devices based on oscillating flapping foils, see, e.g., the review by Xiao & Zhu [1] and the recent work of Belibassakis & Filippas [2], Belibassakis et al. [3], for the extraction and exploitation of this kind of marine renewable resources. Considerable efforts towards the development of biomimetic devices with superior performance have also been made with flexible flapping foils, operating as the main propulsion devices. Such devices show advantages over conventional propellers and have been the subject of several studies over the years, see, e.g., Triantafyllou et al. [4], Shyy et al. [5] and the work of Politis & Tsarsitalides [6]. Prempraneerach & Triantafyllou [7] performed experiments with chord-wise flexible flapping foils in towing tanks, demonstrating their superiority over rigid foils with propulsive efficiencies as high as 87%. Barranyk et al. [8] studied the effects of chord-wise flexibility of flat plates experimentally, reporting that the more flexible plates showed enhanced propulsion characteristics. Paraz et al. in [9], [10] worked towards the theoretical and experimental investigation of the structural response of flexible flat plates under heaving motions, with experiments revealing that the thrust displayed peaks in motion frequency values coinciding with the resonance frequencies of the system comprised of the foil and the surrounding fluid. These experimental results were also used for validating the fully-coupled model for the fluid-structure interaction of chord-wise flexible plates presented in the work of Priovolos et al [11].

Motivated by this aspect of performance enhancement Jeanmonod & Olivier [12] recently performed systematic studies with chord-wise flexible flapping foil energy extraction devices in an effort to tackle this complex fluid-structure interaction problem, revealing that flexible plates can extract up to more than twice the power of the corresponding rigid ones. However, the investigation of this performance enhancement due to the chord-wise flexibility of oscillating foils remains incomplete. Flapping foils have also been studied as wave extraction devices in augmenting the overall ship propulsion by directly converting kinetic energy from ship motions to thrust, see, e.g., De Silva & Yamaguchi [13], Belibassakis & Politis [14], Filippas & Belibassakis [15], Bøckmann & Steen [16].

The present work is focused on the investigation of chord-wise flexible oscillating hydrofoils, examined as biomimetic systems for the extraction of marine renewable energy. The system performs prescribed oscillatory

1738 - Tidal hydrodynamic modelling
All authors share the same affiliation, School of Naval Architecture and Marine Engineering at the National Technical University of Athens, Heroon Polytechniou 9, Zografos 15773, Athens, Greece.
D. E. Anevlavi (email: nm13001@central.ntua.gr).
E. S. Filippas (email: evfilip@central.ntua.gr).
A. E. Karperaki (email: karperaki.ang@gmail.com)
K.A. Belibassakis (email:kbel@fluid.mech.gr)

motions and is free to deform under inertial and reactive forces caused by its motion and hydrodynamic pressure. The hydro-elastic analysis is based on a time domain Boundary Element Method (BEM) for the unsteady lifting flow problem and a high-order Finite Element Method (FEM) for the prediction of the deformed body geometry using the Kirchhoff-Love thin plate theory for cylindrical bending under plane strain conditions. The foil is considered clamped at its leading edge, while its trailing edge acts as a free end. The structural and hydrodynamic aspects of the problem are coupled in an implicit manner, encapsulating forms of non-linearity. Particularly the fluid forcing to the structure that is dependent on the shape of the body boundary, acts as external forcing to the structural equations of motion. To treat the implicit non-linearity we have developed a coupled BEM-FEM numerical scheme.

In this work we focus on the investigation of elasticity effects on the performance of an unsteady flapping-foil thruster. Numerical results are shown and compared against other models and experimental data, validating the present method and illustrating that chord-wise flexibility and flexural rigidity profile variations can significantly improve the propulsive efficiency of the biomimetic thruster. The present method could also serve as a useful tool for the preliminary design and optimum control of flexible biomimetic systems for tidal and wave energy extraction.

II. FORMULATION OF THE HYDRODYNAMIC PROBLEM

In the present work we consider a symmetric foil of infinite span as fully submerged into the surrounding fluid. The 2-D fluid motion is modelled with the assumption of potential flow.

The flow region is an open domain $D \subseteq \mathbb{R}^2$ with time-dependent boundaries assumed to be smooth everywhere except the trailing edge, $\partial D(t) = \partial D_B(t) \cup \partial D_W(t)$. The first component $\partial D_B(t)$ refers to the foil's deformable exterior surface and the latter $\partial D_W(t)$ to the evolution of trailing vortex sheet, with respect to an earth-fixed reference frame, see Figure 1.

A curvilinear body-fixed coordinate system located on $\partial D_B(t)$ and fixed at the foil's centre of rotation along chord length with no inclination is also used to describe the geometry of the foil, in a non-inertial reference frame.

In this formulation the foil is actuated at the centre of rotation and is subjected to a combination of harmonic heaving and pitching motions.

The governing equation for the potential field, i.e. Laplace equation,

$$\nabla^2 \Phi(x,y;t) = 0, \quad (x,y) \in D \tag{1}$$

supplemented by the no-entry boundary condition is,

$$\frac{\partial \nabla \Phi(x,y;t)}{\partial \mathbf{n}_B} = (\mathbf{V}_B - \mathbf{U}_\infty) \cdot \mathbf{n}_B, \quad (x,y) \in \partial \mathrm{D}_B \tag{2}$$

where $\mathbf{n}_B$ denotes the unit normal vector on the body, $\mathbf{U}_\infty$ the free stream velocity and $\mathbf{V}_B$ the instantaneous velocity of the body (due to the oscillatory motions and deformations).

We treat the above as an initial value problem and the disturbance potential Φ and velocity $\nabla\Phi$ vanish at large distance from the body. On the trailing vortex sheet the following kinematic and dynamic conditions hold,

$$\frac{\partial \Phi_W^+(x,y;t)}{\partial n} = \frac{\partial \Phi_W^-(x,y;t)}{\partial n}, \quad (x,y) \in \partial D_W \tag{3}$$

$$p_W^+(x,y;t) = p_W^-(x,y;t), \quad (x,y) \in \partial D_W \tag{4}$$

with superscripts $\{+,-\}$ denoting the upper and lower side of the wake respectively, stating that the pressure p_W and normal velocity $\partial_n \Phi_W$ are continuous through the wake ∂D_W. Using (3) and (4) in conjunction with Bernoulli's theorem we obtain

$$\frac{D\mu_W(x,y;t)}{Dt} = 0, \quad (x,y) \in \partial D_W \tag{5}$$

where $\mu_W = \Phi_W^+ - \Phi_W^-$ denotes the potential jump on the wake and $D/Dt = \partial/\partial t + \mathbf{V}_m \cdot \nabla$ the material derivative based on the mean total velocity $\mathbf{V}_m = 0.5\left(\nabla\Phi_T^+ + \nabla\Phi_T^-\right)$ on the trailing vortex sheet.

Under this approach, ∂D_W evolves in time as a material curve, whose motion is part of the solution. However, in the present study the simplified wake model is used, based on the assumption that the generated vortex curve emanates parallel to the bisector of the trailing edge. Similar wake models have also been described and used in by La Mantia and Dabnichki [17], [18], [19]. This linearization provides satisfactory predictions in cases of low to moderate unsteadiness. Modelling the free wake dynamics as well as its effects on the overall hydrodynamic performance of the deformable foil is left as a subject for future work.

The study of lifting flows around hydrofoils with potential theory requires another condition to be enforced on the trailing edge. In the present work we implement a non-linear, pressure-type Kutta condition that requires the pressure difference at the trailing edge (TE) to be zero,

$$\frac{\partial\left(\Phi^+ - \Phi^-\right)}{\partial t} + \frac{1}{2}\left(\nabla\Phi_T^+ - \nabla\Phi_T^-\right)\left(\nabla\Phi_T^+ + \nabla\Phi_T^-\right) = 0 \tag{6}$$

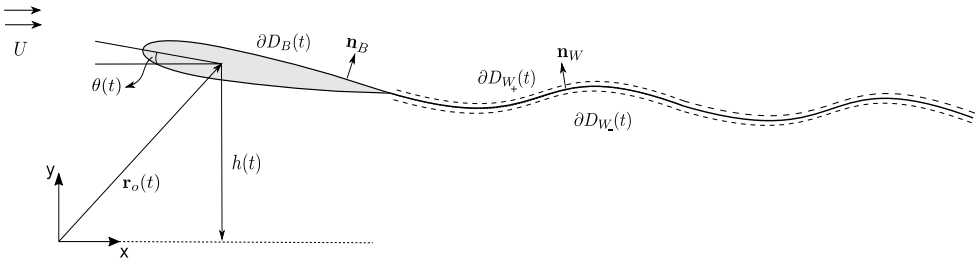

Fig. 1. Biomimetic energy harvesting device based on prescribed kinematics.

Applying the representation theorem, see e.g. Kress [20], to (1)-(4), for every point $\mathbf{x}_0 \in \partial D$ the following boundary integral equation (BIE) is obtained.

$$\frac{1}{2}\Phi_B(\mathbf{x}_0;t) + \int_{\partial D_B(t)} \Phi_B(\mathbf{x};t)\partial_n G(\mathbf{x}_0 \mid \mathbf{x})ds(\mathbf{x}) = \\ = \int_{\partial D_B(t)} \underbrace{\mathbf{V}_B \cdot \boldsymbol{n}_B}_{b\ \mathbf{x};t} G(\mathbf{x}_0 \mid \mathbf{x})ds(\mathbf{x}) - \int_{\partial D_W(t)} \Phi_W\ (\mathbf{x};t)\partial_n G(\mathbf{x}_0 \mid \mathbf{x})ds(\mathbf{x}) \tag{7}$$

$$G(\mathbf{x}_0 \mid \mathbf{x}) = \frac{1}{2\pi}\ln r(\mathbf{x}_0 \mid \mathbf{x}) \tag{8}$$

$$\Phi_W\ = \Phi_W^+ - \Phi_W^- = \mu_W \tag{9}$$

where $G(\mathbf{x}_0 \mid \mathbf{x})$ the fundamental solution of the Laplace equation, $\partial_n G(\mathbf{x}_0 \mid \mathbf{x})$ the directional derivative and μ_W the potential jump or dipole intensity on the wake, i.e. a quantity that changes over time and thus representing the history of circulation and $\mathbf{r}(\mathbf{x}_0 \mid \mathbf{x}) = \{(x_0 - x),(y_0 - y)\}$.

A. Performance parameters

Energy harvesting systems with forced pitching $\theta(t)$ and heaving motions $h(t)$ as shown in Figure 1, are characterized by the cycle-averaged power coefficient, see e.g. [1],

$$C_{op} = \frac{\overline{P}}{1/2\rho U_\infty^3 cs} \tag{10}$$

where ρ is the fluid density, c the chord length of the foil, s is the span length, and $\overline{P}$ is the cycle-averaged power given as

$$\overline{P} = \frac{1}{T}\int_t^{t+T} [L(t)\dot{h}(t) + M(t)\dot{\theta}(t)]dt \tag{11}$$

where $M(t)$ is the instantaneous pitching moment and $L(t)$ the instantaneous lift. The efficiency of energy harvesting device is defined as the ratio of the cycle-averaged power to the incoming flow energy flux,

$$\eta = \frac{\overline{P}}{1/2\rho U_\infty^3 Y_p s} \tag{12}$$

where Y_p is the difference between the highest and lowest points reached by the foil. Moreover, the difference coefficient along the chord length is defined as,

$$\Delta C_P = \frac{p_- - p_+}{\frac{1}{2}\rho U_\infty^2} \tag{13}$$

The non-dimensional pressure coefficient along the body boundary is calculated using Bernoulli's theorem in conjunction with equation (13).

The forces and moments are given below in the form of non-dimensional coefficients for the instantaneous lift, thrust and moment respectively, where $\mathbf{r}(s|s^*;t)$ denotes the reference vector for moment calculation.

$$C_L = \frac{L(t)}{\frac{1}{2}\rho U_\infty^2 c} = \frac{1}{c}\int_{\partial D_B} (\Delta C_p \cdot \mathbf{n}) \cdot \hat{y} ds \tag{14}$$

$$C_T = \frac{T(t)}{\frac{1}{2}\rho U_\infty^2 c} = -\frac{1}{c}\int_{\partial D_B} (\Delta C_p \cdot \mathbf{n}) \cdot \hat{x} ds \tag{15}$$

$$C_M = \frac{M(t)}{\frac{1}{2}\rho U_\infty^2 c^2} = \frac{1}{c^2}\int_{\partial D_B} (\Delta C_p \cdot \mathbf{n}) \cdot \mathbf{r}(s|s^*;t) ds \tag{16}$$

B. Discretization scheme for BEM

Following a low-order discretization scheme the boundary ∂D is decomposed into piecewise linear segments, i.e. the boundary elements. We assume piecewise constant intensity distributions of the fundamental solution

(sources) and its derivative (dipoles) on the boundary. The discretized BIE in equation (7) is as follows,

$$\mathbf{A}\cdot\mathbf{\Phi}_{\mathrm{B}}=\mathbf{S}\cdot\mathbf{b}+\mathbf{W}\cdot\boldsymbol{\mu}_{W}+\mathbf{W}_{K}\mu_{W1} \tag{17}$$

where $\mathbf{A}=\left\{\frac{\delta_{ij}}{2}+B_{ij}\right\}$, $\mathbf{S}=\left\{A_{ij}\right\}$, $\mathrm{i}\in\{1,...\mathrm{N}_B\}$, $\mathrm{j}\in\{1,...\mathrm{N}_B\}$ $\mathbf{W}=\left\{-B_{ik}\right\}$, $\mathbf{W}_K=\left\{-B_{i1}\right\}$, $i\in\{1,...,N_B\}$, $k\in\{2,...,N_W(t)\}$. In the above equations, δ_{ij} is the Kronecker delta, $\mathbf{\Phi}_{\mathrm{B}}=\{\Phi_{B,i}\}$, $\mathbf{b}=\{\partial\Phi_{B,i}/\partial n\}$, $\boldsymbol{\mu}_w=\{\mu_{wk}\}$. In the sequel, we will denote with bold, quantities containing the values of piecewise constant hydrodynamic functions on the panels, at various parts of the boundary. Also for the induced factors it holds,

$$A_{ij}=\int_{panel\ j}G_s(\mathbf{x}_i\,|\,\mathbf{x}_j)dS,\ B_{ij}=\int_{panel\ j}\partial_n G_s(\mathbf{x}_i\,|\,\mathbf{x}_j)dS \tag{18}$$

In the case of straight-line panels, the integrals in (18) have analytic solutions, see e.g. Moran [21] as well as Katz & Plotkin [22]. Multiplying (18) with $\mathbf{A}^{-1}$ we obtain

$$\mathbf{\Phi}_{\mathrm{B}}=\mathbf{D}\cdot\mathbf{b}+\mathbf{P}\cdot\boldsymbol{\mu}_{W}+\mathbf{Z}\mu_{W1}, \tag{19a}$$

$$\mathbf{D}=\mathbf{A}^{-1}\mathbf{S} \tag{19b}$$

where $\mathbf{P}(\mu_W)=\mathbf{A}^{-1}\left(\mathbf{W}\cdot\boldsymbol{\mu}_W\right)$, $\mathbf{Z}=\mathbf{A}^{-1}\mathbf{W}_K$ and $\mathbf{D}$ denotes the Dirichlet-to-Neumann (DtN) operator, that sets a mapping between the boundary values of the potential and their normal derivatives. For more details refer to [23].

In the present work we consider μ_{W1} as the dynamic variable of the problem and thus approaching the solution of an Initial Value Problem (IVP). In order to express the pressure-type Kutta condition as a function of μ_{W1} we substitute equation (19) into (6) and then use the Leibniz rule. In this way we obtain the following non-linear first order differential equation as follows,

$$\frac{d\mathbf{U}}{dt}=\mathbf{f}(\mathbf{U}),\ \mathbf{U}(t_o)=\mathbf{U}_o, \tag{20}$$

$$\begin{aligned}\mathbf{f}(\mathbf{U})=&\left[\frac{-1}{\mathrm{Z}}\frac{d\left(\ \mathrm{Z}\ \right)}{dt}\right]\cdot\mathbf{U}\\&+\left[\frac{-1}{\mathrm{Z}}\frac{d\left(\ \mathbf{D}\ \cdot\mathbf{b}+\ P\ \right)}{dt}\right]+\left[\frac{\mathscr{N}(\mathbf{U})+\mathscr{L}(\mathbf{U})}{\mathrm{Z}}\right],\end{aligned} \tag{21}$$

where $\mathbf{U}=\mu_{W1}$, $\mathbf{f}(\mathbf{U})$ denotes a vector function, $\mathscr{L}(\mu_{W1}),\mathscr{N}(\mu_{W1})$ are linear and non-linear terms from the discretized version of the pressure-type Kutta condition, $\mathbf{D}=\left[\!\left[\{D\}_{ij}\right]\!\right]_{i=1}^{i=N_B}$ is a vector and $P=P_i{}_{\,i=1}^{\,i=N_B}$, $Z=Z_i{}_{\,i=1}^{\,i=N_B}$ are scalars. Notice that Ψ symbolizes the difference of a function Ψ at the trailing edge.

C. *Time integration*

For the numerical solution of the IVP in equations (20) and (21) we implement a higher-order Adams-Bashford-Moulton (A.B.M.) scheme, that provides accuracy, stability and efficiency. The following scheme requires the calculation of only two derivative equations at each time step, and has error of order (Δt^5), where Δt is the time step. More details about the use of this numerical scheme can be found in [23].

III. HYDROELASTIC COUPLING

The foil, as a structural member, is assumed to be a perfectly elastic, homogeneous and isotropic thin elastic plate. The dynamic structural response of the plate is modelled using the classical plate theory (CPT) based on the Kirchhoff-Love hypothesis, see [24] for more details. For the case of cylindrical bending under plane strain assumptions the 2D elasticity problem reduces to an 1D problem.

We consider a body-fixed coordinate system positioned at the leading edge of the foil, such that the x-plane coincides with the geometric mid-plane of the plate and z-axis is pointing upwards. The domain in this formulation is $\Omega\subset\mathbb{R}$ and the plate's fabrication is assumed to be symmetric about the mid-surface.

The governing equation of the initial boundary value problem (IBVP) with respect to the transverse displacement on the mid-plane w_o in $(0,\mathrm{L})\times(0,\mathrm{T})$ is

$$m(x)\frac{\partial^2 w_o(x;t)}{\partial t^2}+\nabla^2[D(x)\nabla^2 w_o(x;t)]=q(x;t) \tag{22a}$$

$$q(x;t)=\frac{1}{2}\rho\mathrm{U}_\infty^2\Delta\mathrm{C}_p \tag{22b}$$

$$D(x)=\frac{Eh(x)^3}{12(1-\nu^2)} \tag{23}$$

where $\Delta\mathrm{C}_p$ denotes the non-dimensional chord-wise pressure difference supplemented by the unsteady hydrodynamic problem described in (13), ν denotes Poisson's ratio, ρ is the material density, $m(x)$ the mass distribution and $D(x)$ the flexural rigidity.

The foil is assumed to be clamped at the pivot point with the leading and trailing edges remaining free from loading. To account for these boundary conditions we consider two thin cantilever plates that share the pivot

point at $x=a$. This point in the structure is assumed to be clamped with zero deflection and slope.

$$w_o(x;t)\big|_{x=a} = \partial_x w_o(x;t)\big|_{x=a} = 0 \tag{24a}$$

Additionally, at the free moving edges, conditions of vanishing moment and shear force are applied, thus assuming the required regularity $D(x)$ it holds that

$$\begin{aligned} D(x)\partial_x^2 w_o(x;t)\big|_{x=0} &= \partial_x[D(x)\partial_x^2 w_o(x;t)]\big|_{x=0} = 0 \\ D(x)\partial_x^2 w_o(x;t)\big|_{x=L} &= \partial_x[D(x)\partial_x^2 w_o(x;t)]\big|_{x=L} = 0 \end{aligned} \tag{24b}$$

supplemented by the following initial conditions suggesting quiescence for the structure,

$$w_o(x;t)\big|_{t=0} = \partial_t w_o(x;t)\big|_{t=0} = 0 \tag{25}$$

The equivalent weak formulation of the IBVP can be derived by multiplying (22a) and (25) by the test functions $\upsilon(x;t)\in \mathrm{H}^2(\Omega)$ and performing integration by parts using the appropriate boundary conditions (24), see [25] for more details. The variational problem is to find w_o so that $\forall \upsilon \in \mathrm{H}^2(\Omega)$,

$$\int_0^L -D(x)\partial_{xx} w_o \partial_{xx}\upsilon dx + \int_0^L m(x)[\partial_{tt} w_o]\upsilon dx = \int_0^L q(x;t)\upsilon dx \tag{26}$$

and $\langle w_o(x,0),\upsilon\rangle\big|_{L^2(\Omega)} = \langle \partial_t w_o(x,0),\upsilon\rangle\big|_{L^2(\Omega)} = 0$ with the $L^2(\Omega)$ inner product notation.

D . *Discretization scheme for FEM*

Out of the standard techniques for partial differential equation solution approximation, we have chosen a finite element approach with 5th order Hermite polynomials Hence, approximate solutions are taken as,

$$w^h = \sum_i^6 w_i^h(t) H_i(x) \tag{27}$$

where $w_i^h(t)$ denotes the time-dependent nodal unknowns and $H_i(x)$ the interpolating Hermite shape functions.

A second order system of ODEs is derived when the approximate solutions (27) are substituted into a discretized equation (26) and the resulting formula is tested only with the shape functions. Using Gaussian quadrature for the numerical integration of quantities appearing in the system of equations we have,

$$\mathbf{M}_{glob}\ddot{U} + \mathbf{K}_{glob}U = \mathbf{F} \tag{28}$$

where $\mathbf{M}_{glob}\in\mathbb{R}^{N_T\times N_T}$, $\mathbf{K}_{glob}\in\mathbb{R}^{N_T\times N_T}$ stand for the global mass and stiffness matrices respectively, $\mathbf{F}_{glob}\in\mathbb{R}^{N_T}$ is the global load vector, $U\in\mathbb{R}^{N_T}$ is the vector containing the nodal unknowns for the partitioned domain Ω^h and N_T refers to the total degrees of freedom (DOFS). Details concerning the numerical implementation of the FEM scheme can be found in Hughes [26]. The addition of the proportional damping terms yields an extended global equation

$$\mathbf{M}_{glob}\ddot{U} + \mathbf{C}\dot{U} + \mathbf{K}_{glob}U = \mathbf{F} \tag{29}$$

$$\mathbf{C} = \alpha_1\mathbf{M}_{glob} + \alpha_2\mathbf{K}_{glob}, \text{ for } \alpha_1,\alpha_2\in\mathbb{R} \tag{30}$$

where α_1,α_2 denote the proportional (or Rayleigh) damping coefficients. In the present work, these coefficients are approximated using the procedure described in [27].

E . Discretization scheme for FEM

The fluid-structure interaction problem contains an implicit non-linearity that is inherent to the passive deformation problem. The forcing term on the RHS of (22a) is dependent on the mid-plane deformation $w_o(x;t)$, which coincides with the foil's camber line, and vice versa. Thus the pressure forcing term (22b) should be formally written as $q(x,t;w_o)$. In the present work, we introduce the following coupling mechanisms between the BEM and the FEM solvers through adjustments in the no-entry boundary condition.

The no-entry boundary condition must include the normal to the un-deformed camber line deformation velocity. This velocity term that is added to the velocities on the boundary of the rigid foil equals to $\partial_t w_o \cdot \mathbf{n}_{rigid}$. The unit normal vector $\mathbf{n}_{rigid} = [-\sin\theta(t),\ \cos\theta(t)]^T$ depends only on the pitching motion. For a similar approach see the recent work by Priovolos et al. [11]. We proceed with implementing order reduction in (30) and deriving the following system of non-linear first order differential equations,

$$\mathbf{A}Q = \mathbf{B}Q + \mathbf{F}, \quad Q = \begin{bmatrix} U & \dot{U} \end{bmatrix}^T \tag{31}$$

where $\mathbf{A} = \begin{bmatrix} \mathbf{0} & \mathbf{M}_{glob} \\ -\mathbf{I} & \mathbf{0} \end{bmatrix}$, $\mathbf{B} = -\begin{bmatrix} \mathbf{K}_{glob} & \mathbf{C} \\ \mathbf{0} & \mathbf{I} \end{bmatrix}$, $\mathbf{F} = \begin{bmatrix} \mathbf{F}_{glob} \\ \mathbf{0} \end{bmatrix}$ and the identity matrix denoted as $\mathbf{I}$ For numerical time integration of (31) we use the Crank-Nicolson time integration scheme,

$$Q(t_{n+1}) = [\mathbf{A} - \mathbf{B}\,{}^{dt}\!/_{2}]^{-1}\left([\mathbf{A} + \mathbf{B}\,{}^{dt}\!/_{2}]Q(t_n) + \mathbf{F}(t_{n+1})dt\right) \tag{32}$$

concluding to the following form of equation (32),

$$\left(\mathbf{A}-\frac{1}{2}\Delta t\cdot\mathbf{B}\right)Q(t_{n+1})-\left(\mathbf{A}+\frac{1}{2}\Delta t\cdot\mathbf{B}\right)Q(t_n)$$
$$-\frac{1}{2}\Delta t[\mathbf{F}(t_{n+1})+\mathbf{F}(t_n)]=0 \tag{33a}$$

The above equation can be put in the following form,

$$\mathbf{G}\left(Q_{n+1}\right)=0 \tag{33b}$$

For the solution of (33b) we use the Newton-Raphson method. After we have determined an initial guess Q_n^0 we recursively approximate the unknown vector with the formula below:

$$Q_{n+1}^q=Q_n^q-\mathbf{J}^{-1}\left(Q_n^q\right)\cdot\mathbf{G}\left(Q_n^q\right),\qquad q=1,2,... \tag{34}$$

where $\mathbf{J}$ is the Jacobian of the function $\mathbf{G}$. The calculation of the Jacobian matrix requires knowledge of the partial derivatives of the scalar components $G_i(Q), i=1,...,N_T$ of the function $\mathbf{G}(Q)$. For the numerical approximation of the partial derivatives we implement a central differences scheme,

$$\frac{\partial G_i}{\partial Q_j}\approx\frac{G_i\left(Q_j+h_j\right)-G_i\left(Q_j-h_j\right)}{2h_j} \tag{35}$$

where h_j is sufficiently small and in practice it is selected as a small percentage of $\left|Q_j\right|$. Therefore, by defining a perturbation vector $\mathbf{h}_n^q=\left[h_1^q,h_2^q,...,h_{2N}^q\right]^T$ we have

$$\mathbf{J}\left(Q_n^q\right)\approx\frac{\mathbf{G}\left(Q_n^q+\mathbf{h}_n^q\right)-\mathbf{G}\left(Q_n^q-\mathbf{h}_n^q\right)}{2\mathbf{h}_n^q} \tag{36}$$

IV. Numerical Results

Regarding the BEM presented in Section II for the hydrodynamic analysis of rigid flapping foils, extensive validation against experimental data as well as numerical calculations concerning the solver's performance over a range of motion parameters, can be found in the work of Filippas & Belibassakis [23]. For the validation of the FEM solver, we performed various comparisons between analytic solutions found in literature and the proposed scheme.

Free vibration analysis of linearly double-tapered cantilever beams with the same taper ratio a, i.e. in terms of horizontal and vertical dimensions, in both axis is presented in the work of Mabie & Rogers [28]. The relative error found for the first five fundamental frequencies, calculated by the present FEM for a mesh of $N_{elem}=15$, is compared against the results in [28] as shown in Table I. The results were in good agreement and they can be further enhanced with refined discretization.

The static behaviour of non-prismatic cantilever beams of length $L=10m$ and maximum thickness $H=0.25m$ under tip load forcing $F=-100kN$ is studied by Beltempo et al. [29]. In Figure 2 we compare the transversal-displacement distributions taken from the literature with the obtained numerical results, confirming once again that they are in good agreement.

TABLE I
MODAL ANALYSIS FOR DOUBLE TAPERED CANTILEVER BEAMS

	Mabie et al. [24]		Relative error with FEM (% x10^{-3})	
Taper ratio	a = 5.0	a = 10.0	a = 5.0	a = 10.0
Ω_1	30.9820	72.0487	0.1451	0.0231
Ω_2	91.9273	186.802	0.0410	0.2007
Ω_3	199.1682	371.238	0.0197	0.1413
Ω_4	356.2088	635.049	0.0198	0.1609
Ω_5	564.1394	981.657	0.0835	0.5628

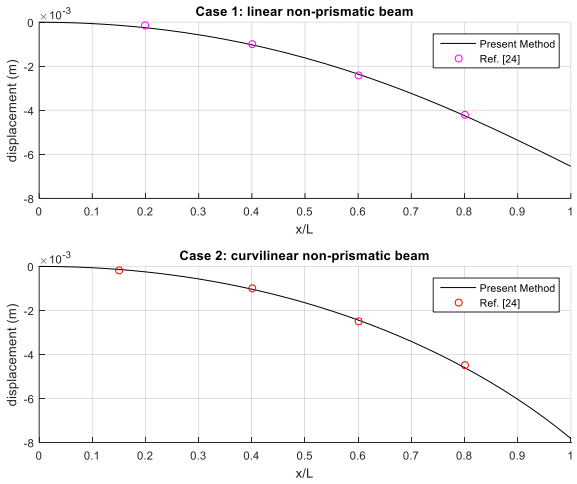

Fig. 2. Static response for non-prismatic beams and comparison with [29]. The transverse displacement is presented as a function of the non-dimensional beam length.

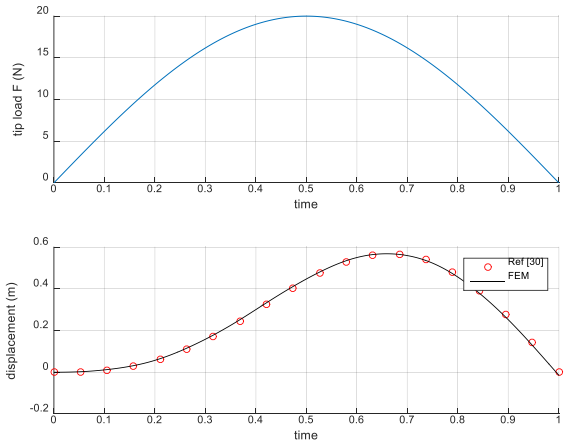

Fig. 3. Dynamic response of the tip of a cantilever beam under tip point load for one period of motion. Comparison against the data published in Warburton [30].

Finally, the FEM solver was validated against a dynamic test case of a cantilever beam of a constant thickness profile, under transverse dynamic tip loading. The beam's response in terms of tip transverse displacement profile is compared in Figure 3 against the analytic solution found in Warburton [30].

F. Comparison of results with experiments in the case of a heaving flexible flapping foil

The most crucial aspect however, is to illustrate the ability of the proposed coupled BEM-FEM to capture the main hydro-elastic effects in the case of chord-wise flexible flapping foils. More specifically we present numerical results simulating an experimental case studied in the work of Paraz et al. [9], for which also analytical predictions were made in [10].

In these series of experiments, the structural response of flexible plates immersed in a uniform flow is studied. The plates are subjected to harmonic heaving motions actuated at their leading edge. As the forcing frequency is gradually increased, resonance peaks are evident in the plates response. We also performed simulations to predict the structural response of the TE when the heaving amplitude is $ho = 0.004$ m, $D = 0.018$ Nm and $U_\infty = 0.05$ m/s. It is important to note that the proportional damping terms used in the simulations were calculated based on the natural frequencies for flat plates immersed in fluid as described in [10]. The mesh used consisted of $N_{BEM} = 120$ panel elements for the BEM solver, $N_{FEM} = 30$ Hermite elements for the FEM solver and $dt/T = 0.005$ for the time discretization, with T referring to the period of the enforced motion.

The numerical results concerning the trailing edge/leading edge response ratios as a function of the normalized forcing frequency are compared against the experimental data in Figure 4. Satisfactory agreement is found between the proposed method and the experimental data, regarding the appearance of the peak and the overall shape of the curve. The small differences, could be attributed to the non-linear damping effects that are not modelled in this work.

Moreover, in the work of Paraz et al. [10] it is highlighted that the structural response of the heaving chord-wise flexible flat plate can be predicted using a linearize d Euler-Bernoulli beam equation that includes non-linear damping terms with emphasis on the transverse drag terms. However, the proposed coupled BEM-FEM numerical scheme is able to predict reasonably well the structural response of the TE using only proportional damping terms.

The deflection envelopes presented Figure 5 are in good agreement with the theoretical results presented in [10]. These deflection envelopes are slightly different from the ones observed experimentally in the work of Paraz et al. [9].

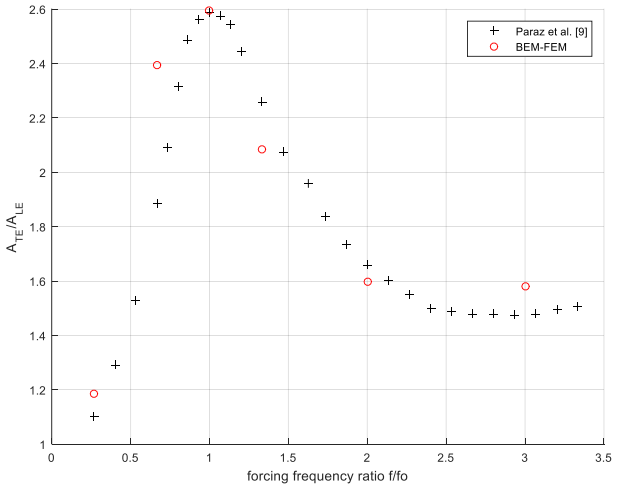

Fig. 4. Trailing edge to leading edge motion amplitude ratio as a function of the normalized forcing frequency for the flexible plate and comparison with experimental data from Paraz et al. [9].

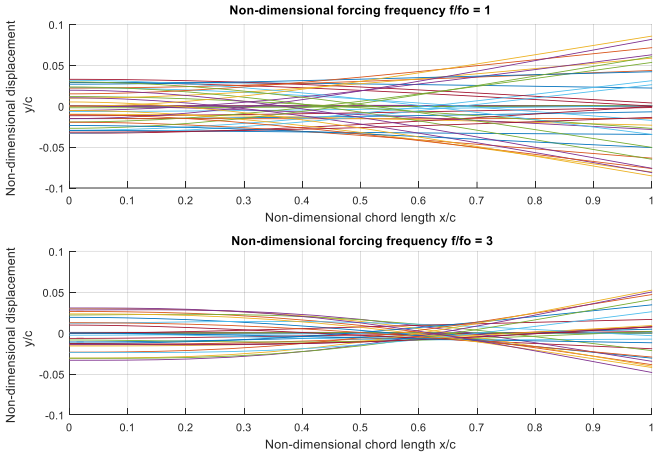

Fig. 5. Deflection envelopes during the last period of motion, with f denoting the frequency of the enforced heaving motion, f_o the first resonance of the system, see. also [9], and c as chord length.

As it has been suggested, fluid-structure interaction models that account for large deformations produce better approximations regarding the structural response of such systems. Motivated by this, extension of the current FEM for large deformation modelling is proposed for future work.

G. Comparison between the rigid and chord-wise flexible flapping device

In this section we present results concerning the fully coupled dynamics of an oscillating foil energy harvesting device, that comes with prescribed kinematics, to illustrate the capabilities of the proposed BEM-FEM numerical scheme. Unlike the simplified plate models with zero thickness, the proposed method can simulate more realistic airfoil shapes, such as the NACA 0012. The

kinematics of the foil in this section are described by harmonic heaving and pitching motions,

$$h(t) = h_o \cos(2\pi ft) \tag{38a}$$

$$\theta(t) = \theta_o \cos(2\pi ft + \varphi) \tag{39b}$$

where $h(t), \theta(t)$ are the instantaneous amplitudes, f is the oscillating frequency; and φ is the phase difference, see Figure 1. The pitch axis is located at $1/3c$ along chord length.

Following recent work of Liu et al [31] we performed simulations concerning an energy harvesting device with the structural characteristics similar to that of polydimethylsiloxane rubbers (PDMS) with material density $\rho = 1200$ kg/m^3, $v = 0.35$ as Poisson's ratio and Young's modulus $E = 0.036 \times 10^7$ Pa. In Figures 6-8 we present numerical results for the structural response of the hydro-mechanical system with non-dimensional heaving amplitude $ho/c = 0.75$, pitch amplitude $\theta_o = 15^o$, free stream velocity $U_\infty = 0.4$ m/s, Strouhal number $St = 2h_o f / U = 0.4$ and phase difference $\varphi = -90^o$. The numerical results were obtained with a mesh of $N_{BEM} = 120$ panel elements, $N_{FEM} = 30$ Hermite elements and time discretization of $dt/T = 0.005$.

Particularly, in Figure 6 we present the time history of camber line deflections on the body-fixed reference frame over the last period of motion. The response amplitude of the trailing edge at $x/L = 1$ is larger compared to that of the leading edge at $x/L = 0$. In this graph we also confirm the correct placement of the pivot point at $1/3c$ along chord length, as the point with zero deflection.

In Figure 7 we present the corresponding time history of pressure difference along chord length that serves as the distributed load for the FEM solver over one period of motion. At the trailing edge positioned at $x/L = 1$, the pressure-type Kutta condition is enforced and therefore pressure difference is zero. Also the highest loading values are observed near the leading edge.

Another interesting aspect of studying the effects of chord-wise flexibility and rigidity profile variations in the analysis of the instantaneous lift, thrust and moment coefficients, is to compare them with the rigid case. Results concerning the performance of rigid hydrofoils can be obtained using only the BEM solver, presented in Section I. In Figure 8, we present such results and we observe reduction of the instantaneous thrust and lift coefficients due to flexibility, whereas the moment coefficient is enhanced. Furthermore, in order to study the effects of chord-wise flexibility and flexural rigidity profile variation on the performance of energy harvesting devices we also performed simulations over a range of design parameters, including Strouhal number and the amplitude of the pitching motion.

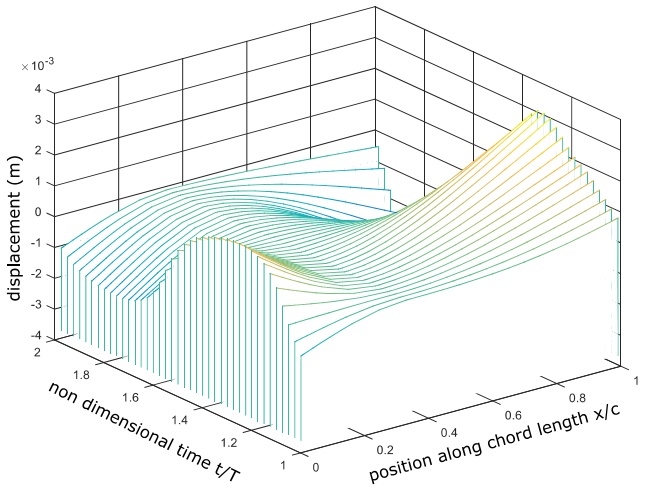

Fig. 6. Camber line deformation time history for the chord-wise flexible foil in flapping motion with $ho/c = 0.75$, $\theta_o = 15^o$, $U_\infty = 0.4$ m/s, $St = 0.4$ over one period of motion.

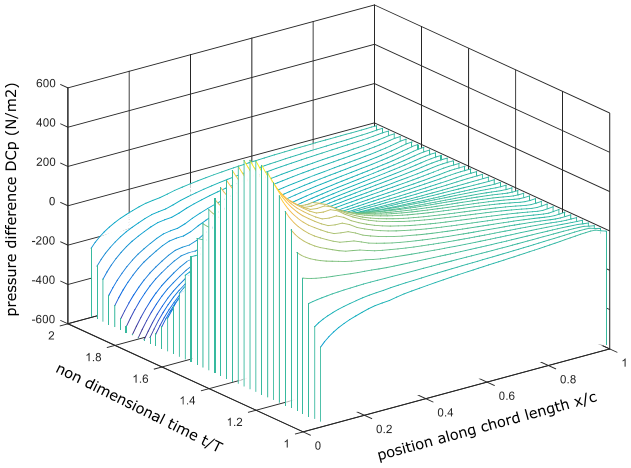

Fig. 7. Chord-wise pressure difference time history for study case $ho/c = 0.75$, $\theta_o = 15^o$, $U_\infty = 0.4$ m/s, $St = 0.4$ over one period of motion.

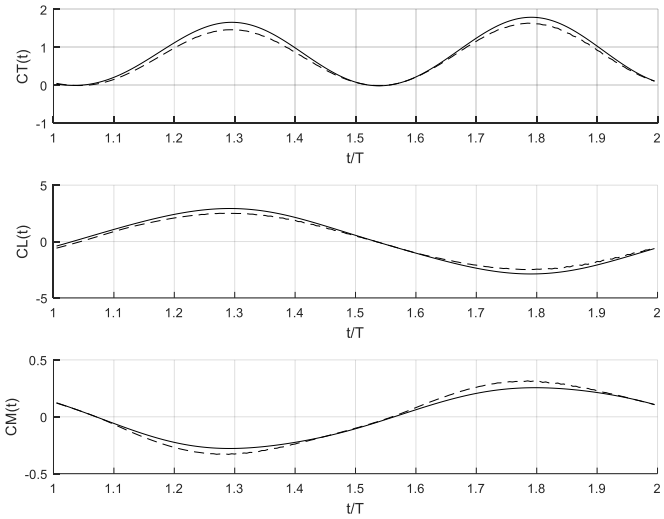

Fig. 8. Instantaneous thrust, lift and moment coefficients (top to bottom) for the flexible (dotted line) and the rigid hydrofoil (solid line) over one period of motion.

In Figures 9-10 we present numerical results concerning the power coefficient and the efficiency of the energy harvesting device respectively as a function of the pitching amplitude for $St = 0.3, 0.35$. In these simulations the foil has chord length $c = 0.1$, material density $\rho = 1200$ kg/m^3, Poisson's ratio $v = 0.35$ and Young's modulus $E = 0.1 \times 10^7$ Pa. The normalized heaving amplitude is $ho/c = 1$, the phase difference $\varphi = -90^o$, and the free stream velocity $U_\infty = 1\, m/s$. The mesh used consisted of $N_{BEM} = 80, N_{FEM} = 15$ elements and a time discretization of $dt/T = 0.004$. In both figures we observe enhancement of the performance parameters due to the effects of flexibility. This enhancement is more evident for large Strouhal numbers. Moreover, an increase of the pitching amplitude leads to evident decrease of both the power coefficient and the efficiency. Finally, in future work the proposed numerical scheme will be extended to treat the more realistic case of a semi-activated chord-wise flexible energy harvesting device with induced heave motions, see Filippas et al. [3].

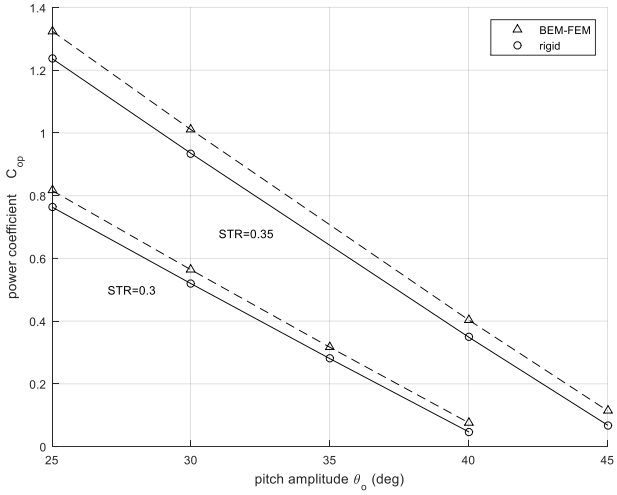

Fig. 9. Power coefficient for the rigid hydrofoil (solid line) compared against the chord-wise flexible foil (dashed line).

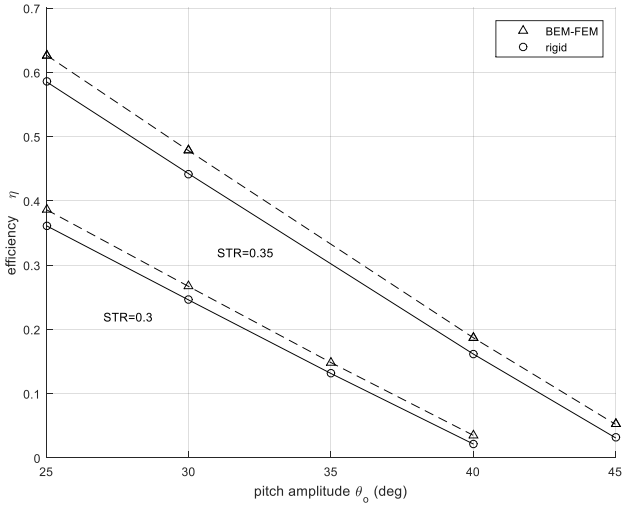

Fig. 10. Efficiency for the rigid hydrofoil (solid line) compared against the chord-wise flexible foil (dashed line).

V. CONCLUSIONS

In this work a model based on potential theory for unsteady hydrodynamics, in conjunction with Kirchhoff-Love plate theory, is developed to study the chord-wise flexibility effects on the performance of biomimetic systems and energy harvesting devices. Numerical results are compared against experimental data for the case of flexible flat plates, in enforced heaving motions, in order to validate the proposed numerical scheme.

Numerical results for a case of flapping foils, with prescribed kinematics, are also presented to highlight the capabilities of the developed BEM-FEM solver. The present model serves as the first step towards the development of a numerical scheme suitable for the prediction of the structural response of a semi-activated energy harvesting device with chord-wise flexibility.

Future work is planned towards the detailed investigation and systematic examination of the structural response of the chord-wise flexible foil over a range of design and operation parameters, including reduced frequency, heaving and pitching amplitudes and effective angle of attack, and various flexural rigidity profiles inspired by nature. Also, special attention will be paid to further validate and examine the applicability range of the proposed scheme through comparison with other numerical methods and experiments found in literature. Direct extensions include the introduction and modelling of various nonlinearities associated with the evolution of the trailing vortex sheet and large deflections in the structural response. Future research also includes the treatment of the 3dimensional deformable flapping wing, including also span-wise flexibility effects.

ACKNOWLEDGEMENT

Support provided to E. S. Filippas by Alexander S. Onassis Benefit Foundation scholarship program.

REFERENCES

[1] Q. Xiao and Q. Zhu, "A review on flow energy harvesters based on flapping foils," *Journal of Fluid and Structures 46*, pp. 174-191, 2014.

[2] K. Belibassakis and E. Filippas, "Biomimetic energy devices in waves and sheared currents," in *2nd International Conference on Renewable Energies Offshore (RENEW2016)*, 2016.

[3] E. S. Filippas, T. P. Gerostathis and K. A. Belibassakis, "Semi-activated oscillating hydrofoil as a nearshore biomimetic energy system in waves and currents," *Ocean Engineering 154*, pp. 396-415, 2018.

[4] M. S. Triantafyllou, G. S. Triantafyllou and D. K. P. Yue, "Hydrodynamics of fishlike swimming," *Annu. Rev. Fluid. Mech*, pp. 32:33-53, 2000.

[5] H. A. C.-K. K. H. L. Wei Shyy, An Introduction to Flapping Wing Aerodynamics, Cambridge University Press, 2013.

[6] G. Politis and V. Tsarsitalidis, "Flexible Oscillating Duct: An approach to a novel propulsor," *Applied Ocean Research, Volume 36,* pp. 36-50, 2012.

[7] P. Prempraneerach, F. S. Hover and M. S. Triantafyllou, "The effect of chordwise flexibility on the thrust and efficiency of a flapping foil," 2013.

[8] O. Baranyyk, B. J. Buckham and P. Oskai, "On the performance of oscillating plate underwater propulsion system with variable chordwise flexibility at differenet depths of submergence," *Journal of Fluids and Structures,* 2010.

[9] F. Paraz, C. Eloy and L. Schouveiler, "Experimental study of the response of a flexible plate to a harmonic forcing in a flow," *Comptes Rendus Mecanique,* pp. 342, 532-538, 2014.

[10] F. Paraz, L. Schouveiler and C. Eloy, "Thrust generation by a heaving flexible foil: Resonance, nonlinearities and optimality," *Physics of Fluids,* January 2016.

[11] A. K. Priovolos, E. S. Flippas and K. A. Belibassakis, "A vortex-based method for improved flexible flapping-foil thruster performance," *Engineering Analysis with Boundary Elements 95,* pp. 69-84, 2018.

[12] G. Jeanmonod and M. Olivier, "Effects of chordwise flexibility on 2D flapping foils used as an energy extraction device," *Journal of Fluids and Structures 70,* pp. 327-345, 2017.

[13] D. Silva and H. Yamaguchi, "Numerical Study on active wave devouring propulsion," *Journal of Marine Science and Technology,* vol. 17, no. 3, pp. 261-275, 2012.

[14] G. K. Politis and K. A. Belibassakis, "Hydrodynamic performance of flapping wings for augmenting ship propulsion in waves," *Ocean Engineering,* vol. 72, pp. 227-240, 2013.

[15] E. S. Filippas and K. A. Belibassakis, "Hydrodynamic analysis of flapping-foil thrusters operating beneath the free surface and in waves," *Engineering Analysis with Boundary Elements 41,* pp. 47-59, 2014.

[16] E. Bøckmann and S. Steen, "Model test and simulation of a ship with wavefoils," *Applied Ocean Research,* vol. 57, pp. 8-18, 2016.

[17] M. L. Mantia and P. Dadnichki, "Unsteady panel method for flapping foil," *Engineering Analysis with Boundary Elements,* vol. 33, no. 4, pp. 572-580, 2009.

[18] M. L. Mantia and P. Dabnichki, "Influence of the wake model on the thrust of oscillating foil," *Engineering Analysis of Boundary Elements,* vol. 35, no. 3, pp. 404-414, 2011.

[19] M. L. Mantia and P. Dabnichki, "Structural response of oscillating foil in water," *Engineering Analysis with Boundary Elements,* vol. 37, no. 6, pp. 957-966, 2013.

[20] R. Kress, Linear integral equations, Springer, 1989.

[21] J. Moran, An introduction to theoretical and computational aerodynamics, New York: J. Wiley & Sons, 1984.

[22] J. Katz and A. Plotkin, Low speed aerodynamics, New York: McGraw-Hill, 1991.

[23] E. S. Filippas and K. A. Belibassakis, "Hydrodynamic analysis of flapping-foil thrusters operating beneath the free surface and in waves," *Engineering Analysis with Boundary Elements* , vol. 41, pp. 47-59, 2014.

[24] J. N. Reddy, Theory and Analysis of Elastic Plates and Shells, CRC Press Taylor & Francis Group, 2007.

[25] I. M. Gelfand and S. V. Fomin, Calculus of Variations, Englewood Cliffs, New Jersey: Prentice-Hall INC., 1963.

[26] T. J. R. Hughes, The Finite Element Method: Linear Static and Dynamic Finite Element Analysis, Englewood Cliffs, New Jersey: Prentice-Hall INC. , 1987.

[27] I. Chowdhury and S. Dasgupta, "Computation of Rayleigh Damping Coefficients for Large Systems," *Electronic Journal of Geotechnical Engineering,* vol. 43, pp. 6855-6868, 2003.

[28] H. H. Mabie and C. B. Rogers, "Transverse vibrations of double-tapered cantilever beams with end support and with end mass," *The Journal of the Acoustical Society of America,* vol. 55, pp. 986-991, 1974.

[29] A. Beltempo, G. Balduzzi, G. Alfano and F. Auricchio, "Analytical derivation of a general 2D non-prismatic beam model based on the Hellinger-Reissner principle," *Engineering Structures,* vol. 101, pp. 88-98, 2015.

[30] G. B. Warburton, The Dynamic Behaviour of Structures, p. 131: Pergamon Press, 1976.

[31] W. Liu, Q. Xiao and Q. Zhu, "Passive Flexibility Effect on Oscillating Foil Energy Harvester," *AAIA Journal,* vol. 54, no. 4, pp. 1172-1187, 2016.

[32] K. Belibassakis, E. Filippas and G. Th. P, "Biomimetic Systems Operating as Marine Energy Devices in Waves and Sheared Currents," in *11th HSTAM International Congress on Mechanics,* Athens, 27-30 May, Greece, 2017.

[33] D. Read, F. S. Hover and M. S. Triantafyllou, "Forces on oscillating foils for propulsion and maneuvering," *Journal of Fluids and Structures,* vol. 17, pp. 163-183, 2003.

[34] L. Schouveiler, F. S. Hover and M. S. Triantafyllou, "Performance of flapping foil propulsion," *Journal of Fluids and Structures,* vol. 20, pp. 949-959, 2005.